



NRC Publications Archive Archives des publications du CNRC

pH-triggered release of hydrophobic molecules from self-assembling hybrid nanoscaffolds

Lu, Lei; Unsworth, Larry D.

This publication could be one of several versions: author's original, accepted manuscript or the publisher's version. / La version de cette publication peut être l'une des suivantes : la version prépublication de l'auteur, la version acceptée du manuscrit ou la version de l'éditeur.

For the publisher's version, please access the DOI link below. / Pour consulter la version de l'éditeur, utilisez le lien DOI ci-dessous.

Publisher's version / Version de l'éditeur:

<https://doi.org/10.1021/acs.biomac.6b00040>

Biomacromolecules, 17, 4, pp. 1425-1436, 2016-03-03

NRC Publications Record / Notice d'Archives des publications de CNRC:

<https://nrc-publications.canada.ca/eng/view/object/?id=9e4287db-e138-42bd-a2f4-805f4418351b>

<https://publications-cnrc.canada.ca/fra/voir/objet/?id=9e4287db-e138-42bd-a2f4-805f4418351b>

Access and use of this website and the material on it are subject to the Terms and Conditions set forth at

<https://nrc-publications.canada.ca/eng/copyright>

READ THESE TERMS AND CONDITIONS CAREFULLY BEFORE USING THIS WEBSITE.

L'accès à ce site Web et l'utilisation de son contenu sont assujettis aux conditions présentées dans le site

<https://publications-cnrc.canada.ca/fra/droits>

LISEZ CES CONDITIONS ATTENTIVEMENT AVANT D'UTILISER CE SITE WEB.

Questions? Contact the NRC Publications Archive team at

PublicationsArchive-ArchivesPublications@nrc-cnrc.gc.ca. If you wish to email the authors directly, please see the first page of the publication for their contact information.

Vous avez des questions? Nous pouvons vous aider. Pour communiquer directement avec un auteur, consultez la première page de la revue dans laquelle son article a été publié afin de trouver ses coordonnées. Si vous n'arrivez pas à les repérer, communiquez avec nous à PublicationsArchive-ArchivesPublications@nrc-cnrc.gc.ca.



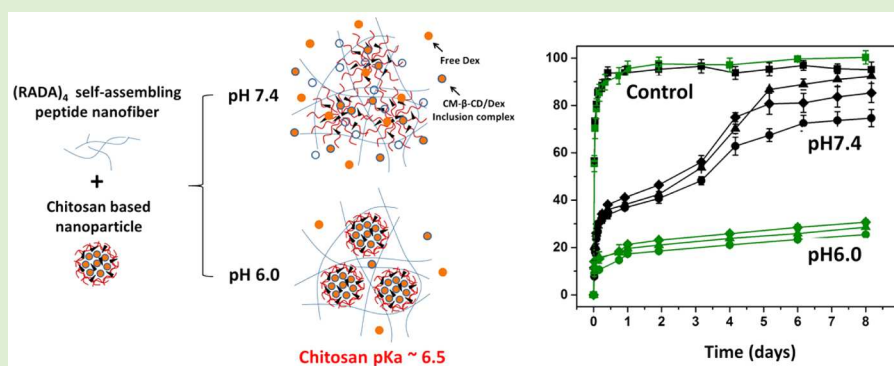
pH-Triggered Release of Hydrophobic Molecules from Self-Assembling Hybrid Nanoscaffolds

Lei Lu^{†,‡} and Larry D. Unsworth^{*,†,‡}

[†]Department of Chemical and Materials Engineering, University of Alberta, Edmonton, Alberta T6G 2V4, Canada

[‡]National Institute for Nanotechnology, National Research Council (Canada), Edmonton, Alberta T6G 2M9, Canada

S Supporting Information



ABSTRACT: Self-assembling peptide based hydrogels have a wide range of applications in the field of tissue repair and tissue regeneration. Because of its physicochemical properties, (RADA)₄ has been studied as a potential platform for 3D cell culture, drug delivery, and tissue engineering. Despite some small molecule and protein release studies with this system, there is a lack of work investigating the controlled release of hydrophobic compounds (i.e., anti-inflammatory, anticancer, antibacterial drugs, etc.) that are important for many clinical therapies. Attempts to incorporate hydrophobic compounds into self-assembling matrices usually inhibited nanofiber formation, rather resulting in a peptide–drug complex or microcrystal formation. Herein, a self-assembling chitosan/carboxymethyl-β-cyclodextrin nanoparticle system was used to load dexamethasone, which formed within a self-assembling (RADA)₄ nanoscaffold matrix. Nanoparticles dispersed within the matrix were stabilized by the nanofibers within. The *in vitro* release of dexamethasone from the hybrid system was observed to be pH sensitive. At pH 7, release was observed for more than 8 days, with three distinct kinetic domains in the first 6 days. Data suggest that the deprotonation of chitosan at a solution pH > 6.8 leads to nanoparticle dissociation and ultimately the release of dexamethasone from the hybrid system. This system has the potential to form a multifunctional scaffold that can self-assemble with the ability to control the release of hydrophobic drugs for a wide variety of applications.

1. INTRODUCTION

Nanoscaffolds formed via peptide self-assembly have the potential for becoming robust drug delivery platforms and, as such, are actively being investigated for regenerative medicine applications.^{1–3} A controlled release system for the delivery of hydrophobic molecules is crucial for anti-inflammatory, antimicrobial, and antitumor therapies.^{4–7} Compared to systemic administration, the localized administration of drugs at the site of interest can result in reduced side-effects, a greater therapeutic outcome, while using a lower overall amount of drug. The ion-complementary self-assembling peptide, (RADA)₄, is composed of alternating hydrophobic and hydrophilic amino acids and has been shown to form well-ordered nanofibers that subsequently develop into a highly hydrated (>99.5% water), three-dimensional nanostructured matrix in physiological solution.^{8–10} In addition, an advantage of peptide self-assembly is the potential for molecular level programmability; biofunctionality of the assembled nano-

scaffold can be introduced by directly altering the self-assembling peptide sequence with functional motifs (e.g., cell adhesion,¹¹ angiogenesis,^{12–14} bone regeneration,^{15,16} nerve regeneration,^{17,18} etc.). Several authors have reported various protein and hydrophilic small molecule release from these nanoscaffolds, including BFGF, VEGF, and BDNF,^{19,20} human antibodies,²¹ where protein release depended primarily on the size of the protein and network density of nanofibers. Sustained release of smaller dye molecules that contain sulfonic acid groups from (RADA)₄ nanoscaffolds have been reported;²² however, few studies have reported the delivery of uncharged hydrophobic small molecules via this type of system.

Although the alanine side chains of (RADA)₄ are hydrophobic and thought to drive assembly through interpeptide

Received: January 12, 2016

Revised: February 23, 2016

Published: March 3, 2016

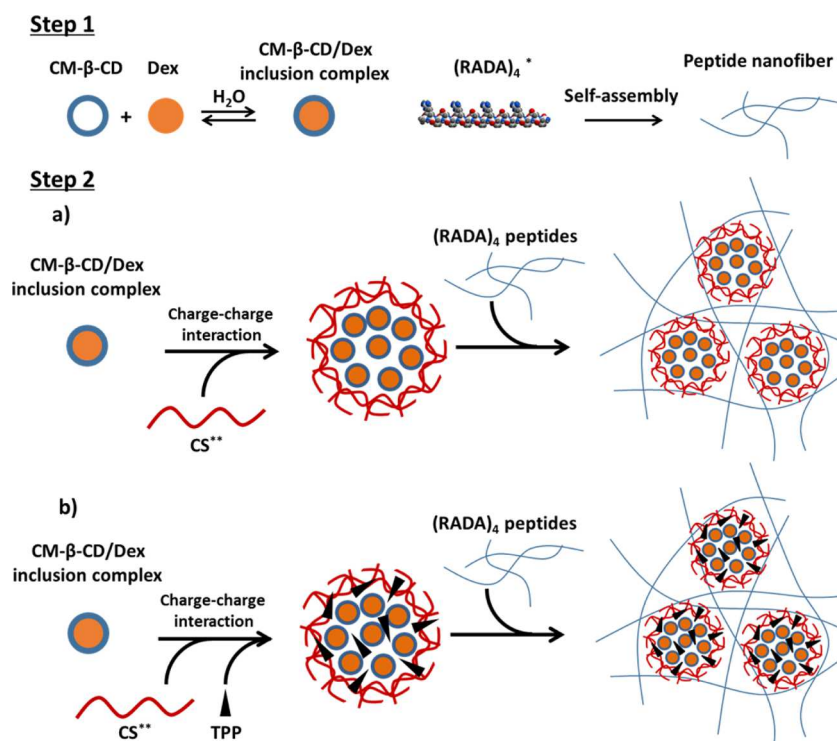


Figure 1. Schematic of the formation process of nanoparticle–nanofiber matrix. (a) Particle without TPP or CS/CM-β-CD/Dex; (b) add TPP as cross-linker or CS/CM-β-CD/Dex/TPP. *, Molecular diagram;⁸ **, CS was dissolved in 1% v/v acetic acid, pH 4.9.

hydrophobic interactions, direct encapsulation of hydrophobic molecules within the hydrophobic phase of the resulting β -sheet is hard. Several hydrophobic anticancer drugs (e.g., paclitaxel,²³ ellipticine,^{24,25} curcumin,²⁶ etc.) have been attempted to be released by (RADA)₄ or other similar ion-complementary self-assembling peptides (e.g., EAK16-IV, EAK16-II and EFK-II,^{24,27–29} MAX8,^{30,31} etc.). However, the usual result of these attempts is either an inhibited nanofiber formation (significant decrease in β -sheet content)²³ or an inability to form nanofiber networks at all: most result in a peptide-drug/microcrystal complex.^{24,25,29} Only the incorporation of curcumin using a MAX8 peptide-based matrix has been shown to allow for stable nanofiber networks, which was thought to be a result of the special folding ability of this peptide sequence.²⁶ To achieve the hydrophobic drug loading without affecting the secondary structure of nanofiber backbones, a two-step strategy of embedding self-assembling nanoparticles loaded with the hydrophobic drug into the nanofiber matrix was explored.

Nanocarriers including nanoparticles, micelles, dendrimers, liposomes, etc., with abundant hydrophobic domains, are commonly used to encapsulate hydrophobic compounds.^{32–34} Composite hydrogels of microspheres, liposomes, and other types of particle-based drug delivery vehicles have been shown to have the capacity for hydrophobic drug release.^{4,35} In this work, we propose a strategy that two kinds of nanostructures, chitosan/cyclodextrin nanoparticles and (RADA)₄ peptide nanofibers, were self-assembled independently and then incorporated into a hybrid nanoscaffold.

Nanoparticles made of chitosan (CS) and carboxymethyl- β -cyclodextrin (CM- β -CD) or mixtures of CM- β -CD/tripolyphosphate (TPP) were used to form stabilized nanoparticles via the ionotropic gelation progress.³⁶ This nanoparticle system has been used to encapsulate drugs with different physicochemical

properties (i.e., hydrophilic and hydrophobic) including insulin,^{36,37} heparin,³⁶ sulindac³⁸ and gene/DNA,³⁹ etc. The pK_a of the amine group in CS is \sim 6.5; thus, the CS-based nanoparticles may dissociate at physiological condition (pH 7.4), a trait that may significantly limit their use in systemic applications.^{36–38} However, this inherent property is suited for inclusion in a (RADA)₄ hydrogel, as this matrix can assemble in acidic environments (\sim pH 4.0,⁴⁰) and formed nanofibers may stabilize the embedded nanoparticle structure allowing for a reduced rate of dissociation upon changing the environmental pH. Cyclodextrins (CDs) are a family of compounds composed of $-(1, 4)$ linked glucopyranose subunits bound together to form a cyclic oligosaccharide. Because of the stereochemical structure, cyclodextrins have an internalized nonpolar cavity that allows for a hydrophobic molecule to be bound, while a hydrophilic exterior allows for this complex to remain soluble in water.⁴¹ CDs can form reversible inclusion complexes with hydrophobic molecules, yielding an improved aqueous solubility and bioavailability of hydrophobic drugs. In this work, the anionic CM- β -CD was selected because it can not only spontaneously interact with the cationic CS, but also can load dexamethasone as inclusion complexes.

Dexamethasone (Dex), a glucocorticoids, is the gold-standard anti-inflammatory medicine due to its high potency and effectiveness in reducing inflammation through binding glucocorticoid receptors.⁴² Dex has been chosen as a model drug for this study due to its widespread use, safety, hydrophobic nature, similarity to other hydrophobic drugs in structure, and relatively complete characterization. Furthermore, it has already been shown that the aqueous solubility of Dex (\sim 0.1 mg/mL) has been enhanced by the pharmaceutical industry for decades using cyclodextrins.⁴³ In this report, the release of Dex from (RADA)₄ based composite matrices was achieved using a CM- β -CD/Dex based nanoparticle that was

mixed with self-assembling peptides to form a hybrid nanoscaffold. The influence of incorporating these nanoparticles on the matrix morphology was also evaluated.

2. MATERIALS AND METHODS

2.1. Materials. CS (degree of deacetylation 96.5%; viscosity 55 mPa.s) was purchased from Yuhuan Ocean Biochemical (Zhejiang, China). Dex, CM- β -CD (the average degree of substitution, DS \sim 3), β -CD, and TPP were purchased from Sigma (USA). (RADA)₄ peptide (\geq 95% purity) was purchased from RS Synthesis (Louisville, KY, USA). The chemical structures of CS, CM- β -CD, TPP, and Dex are shown in Figure S1.

2.2. Nanoparticle Preparation. Nanoparticles, with or without the anionic cross-linker TPP, were prepared according to a modified procedure from the literature (Figure 1).⁴⁴ Briefly, CS was dissolved at 0.2% w/v (2 mg/mL) with 1% v/v acetic acid and then raised to pH 4.9 with 5 N NaOH. Dex/CM- β -CD inclusion complex solution was obtained by dissolving Dex in CM- β -CD water solution via an overnight stirring. For Dex-loaded nanoparticles, 200 μ L of CM- β -CD/Dex solution (CM- β -CD, 9 mg/mL or \sim 6.545 mM; Dex, 0.8 mg/mL or 2.038 mM) and 100 μ L of TPP water solutions (0, 1, 2 mg/mL) were added to 800 μ L of CS solution (0.2% w/v, pH 4.9) under magnetic stirring for 30 min at room temperature. The nanoparticles were isolated by centrifugation in a glycerol bed (20 000 \times g, 30 min, at room temperature) and then resuspended in 100 μ L of Milli-Q water. Glycerol was used for centrifugation to enhance the resuspendability of centrifuged nanoparticles, as described previously.³⁶

The production yield of the nanoparticles was obtained by centrifuging fixed volume of the nanoparticle suspensions (20 000 \times g, 30 min, at room temperature) without glycerol bed. After centrifugation, the supernatant was discarded, the tube with isolated particles at bottom was carefully raised with water, and then it was kept at 60 $^{\circ}$ C in vacuum until constant weight. The production yields were calculated from the ratios between actual weight and the theoretical weight of the nanoparticles.

2.3. Particle Characterization. **2.3.1. Nanoparticle Size and ζ -Potential.** The size and ζ -potential of the nanoparticles in various pH conditions (pH 3.0–9.5; size, 1 \times PBS; ζ -potential, 10 mM KCl) were measured using the Malvern Zetasizer Nano-S (Malvern Instruments, UK).

2.3.2. Fourier Transform Infrared Spectroscopy (FT-IR). In FT-IR analysis, transmittance spectra of KBr sample pellets of pure CS, CM- β -CD, TPP, and dried nanoparticle were obtained using the FT-IR spectrometer (Varian FTS 7000, USA), operating from 4000–500 cm^{-1} at resolution of 2 cm^{-1} .

2.3.3. Drug Loading Capacity of Nanoparticles. The Dex loading and association efficiencies of the nanoparticle preparations were determined after isolation of nanoparticles by centrifugation as described in section 2.2. The amount of loaded Dex in nanoparticles was determined by extracting Dex by incubation and sonication in 50% methanol. Briefly, 50 μ L of the nanoparticle stock solution was added into 1 mL of 50% methanol, incubated overnight at 37 $^{\circ}$ C, then sonicated for 2 h. The above incubation and sonication procedure was repeated to get a sufficient dissolution of Dex. After that, the extract solution was collected after a centrifugation progress (20 000 \times g, 30 min, at room temperature), and the concentration of it was determined by UV–vis at 240 nm; the standard curve was made by pure Dex in 50% methanol.

The loading efficiency and the association efficiency of Dex were calculated as presented below:

$$\text{Yield} = \frac{\text{Nanoparticles weight}}{\text{Total amount of materials}} \times 100 \quad (1)$$

$$\text{Loading efficiency} = \frac{\text{Amount of bound Dex}}{\text{Nanoparticles weight}} \times 100 \quad (2)$$

$$\text{Association efficiency} = \frac{\text{Amount of bound Dex}}{\text{Total amount of Dex}} \times 100 \quad (3)$$

2.3.4. Stability Study of Nanoparticles in Different pH. The stability of particle size in different pH has also been studied. Nanoparticles were incubated in PBS buffer (pH 7.4 or pH 6.0 that chitosan should be protonated, $\text{pK}_a \approx 6.5$) at 37 $^{\circ}$ C. At appropriate time points, samples were collected, and the size distribution of the nanoparticles was measured as described in section 2.3.1.

2.4. In Vitro Dex Release from Nanoparticles. Dex release studies were performed by incubating 50 μ L of NP suspension in 950 mL of PBS buffer (pH 7.4 or pH 6.0) at 37 $^{\circ}$ C. At appropriate intervals, the supernatants of samples were separated and collected by centrifugation (20 000 \times g, 30 min, at room temperature) and then mixed 1:1 with 50% methanol. The amount of released Dex was evaluated by measuring the mixtures by UV–vis at 240 nm (samples without drug were used as a blank), and the standard curve was made by CM- β -CD/Dex inclusion complex solution measured in the same way.

2.5. Atomic Force Microscopy (AFM). The morphology of the hybrid hydrogel matrices and nanoparticles was measured using Dimension 3100 Nanoman atomic force microscopy (AFM, Veeco Metrology, LLC) with tapping mode, tip radius of 8 nm. Nanoparticles stock solutions were 100-times diluted with Mili-Q water, and hydrogel solutions used in AFM studies were prepared by being 500-times diluted with Mili-Q water. A drop (5 μ L) of each solution was placed on freshly cleaved mica substrates then rise with water. The surfaces were air-dried overnight at room temperature before being imaged.

2.6. Circular Dichroism (CD) Measurement. The effect of nanoparticle presence on peptide self-assembly was investigated using CD spectroscopy of 0.5% w/v or 2.92 mM peptide solutions in 5 mM PB, pH 4.0 at 25 $^{\circ}$ C. Briefly, 100 μ L of each nanoparticle stock solutions was made by diluting 16.7 μ L of 3% w/v (RADA)₄ peptide solution with 5 μ L of 100 mM PB and appropriate amount of nanoparticles suspensions and water, incubated at 4 $^{\circ}$ C overnight. The final concentrations of nanoparticle stock solutions were 25%, 50%, and 75% v/v, respectively. CD data were collected by Jasco J-810 Circular Dichroism Chiroptical Spectrometer using a quartz cuvette with a 0.1 mm path length. The effects of the nanoparticles on peptide structure were determined by taking CD scans in different solutions. A background spectrum was first collected for each sample using same concentration of PB or nanoparticle suspensions. All CD measurements were repeated at least three times from 185–260 nm. The raw data were corrected by conversion to mean residue ellipticity. Secondary structure fractions of different formula were estimated from the CD spectra using the free software CDNN 2.1.⁴⁵ The “ β /TR ratio ((β -sheet content)/(β -turn + random coil content))” was used to evaluate and speculate the quality of hydrogels from a secondary structure level.

2.7. In Vitro Dex Release from Hydrogel–Nanoparticle Composite. In this study, on the basis of the CD result, we select 0.5% w/v (RADA)₄ with 25% v/v of nanoparticle stock solutions for in vitro drug release. Similarly to CD sample preparation, (RADA)₄ solution was diluted with 5 mM PB buffer and mixed with the nanoparticle suspension to obtain desired concentrations. Thirty microliters of the mixture was placed at the bottom of a vial insert (150 μ L) in a 1.5 mL vial overnight at 4 $^{\circ}$ C. Then 120 μ L of PBS (pH 7.4 or 6.0) was carefully added to each vial insert. The samples were incubated at 37 $^{\circ}$ C. The control groups of Dex passive release without nanoparticles was represented by mixing (RADA)₄ peptide with same concentration of CM- β -CD/Dex solution (assuming the average drug association efficiency of nanoparticles is 20%). At each time point, 80 μ L of supernatant was taken out and replaced by fresh PBS to maintain a sink condition. The amount of released Dex was determined by UV–vis at 240 nm as the method described in section 2.4.

2.8. Statistical Analysis. All data were presented as means \pm standard deviation (SD). The statistical significance of differences between mean values was determined using one-way ANOVA followed by Student's *t* test for analysis of variance. Significance was established by a value of $p < 0.05$.

Table 1. Loading Characteristics of Dex Loaded Nanoparticles with Different Ratios of CS/CM- β -CD/Dex/TPP. Data Presented Represent the Mean \pm SD for $n \geq 3$

sample	ratio CS/CM- β -CD/Dex/TPP	yield (%)	Dex loading efficiency (%)	association efficiency (%)
TPP-0	4:4.5:0.4:0	34 \pm 7	2.3 \pm 0.2	17.4 \pm 1.7
TPP-0.25	4:4.5:0.4:0.25	41 \pm 3	2.1 \pm 0.3	20.7 \pm 2.2
TPP-0.5	4:4.5:0.4:0.5	55 \pm 1	1.9 \pm 0.1	24.1 \pm 0.9

3. RESULTS

3.1. Nanoparticle Preparation. It has been previously reported that a narrow range of ratios of CS/CM- β -CD or CS/CM- β -CD/TPP concentration ultimately yields nanoparticles, where the concentration of CM- β -CD or TPP dictates the ability to form nanoparticles versus large aggregates that cannot be resuspended in solution.³⁶ For this study, several formulas were screened for their ability to load Dex (results not shown), of which only three were chosen for further study as they were able to be resuspended after centrifugation and exhibited a relatively high loading efficiency (Table 1).

3.2. Nanoparticle Characterization. **3.2.1. FT-IR.** Control materials were characterized using FT-IR spectroscopy (Figure 2), where pure TPP (Figure 2a) showed characteristic bands at

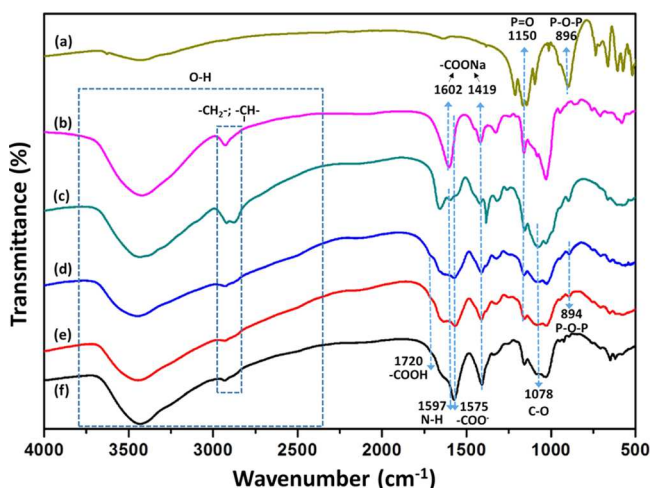


Figure 2. Representative FT-IR spectra for (a) TPP, (b) CM- β -CD, (c) CS, and nanoparticles: (d) TPP-0.5, (e) TPP-0.25, (f) TPP-0.

1150 (P=O stretching vibrations) and 896 cm^{-1} (P-O-P asymmetric stretching).^{46,47} All other remaining spectra showed a broad O-H stretch peak at $\sim 3425 \text{ cm}^{-1}$ and peak at $\sim 2900 \text{ cm}^{-1}$ for the C-H stretch. CM- β -CD sodium salt (Figure 2b) had bands at 1419 and 1602 cm^{-1} corresponding to the symmetrical and asymmetrical stretching vibration of the carboxylate groups, respectively. Virgin CS (Figure 2c) showed bands at 1078 and 1597 cm^{-1} for the C-O stretching for a primary -OH and N-H deformation of amine groups, respectively.

Nanoparticles (Figure 2d-f, TPP-0.5, TPP-0.25, and TPP-0) were also characterized using FT-IR. The main differences in the FT-IR spectrum among those nanoparticles relate to the spectrum of raw CS and refer to the strong characteristic bands at 1419 and 1575 cm^{-1} . These bands correspond to the symmetrical and asymmetrical stretching vibrations of the -COO⁻ groups, where the peak at 1602 cm^{-1} (-COONa) for raw CM- β -CD shifted to 1575 cm^{-1} (-COO⁻) upon nanoparticle formation. In addition, a weak band at 1720 cm^{-1} could be assigned to the stretching vibration of carboxyl group. A band at $\sim 1150 \text{ cm}^{-1}$ that is associated with the P-O stretching vibration of TPP is present in the nanoparticle spectra; however, it is overlapped by a strong peak also present for the abundant CS. Another characteristic band for TPP presence was observed at 894 cm^{-1} for nanoparticles with TPP-0.5 and TPP-0.25 (Figure 2d,e).⁴⁸ These data show that all three components are found within the formed nanoparticles.

3.2.2. Nanoparticle Characterization: Effect of pH. Dex-loaded nanoparticle size and ζ -potential were significantly affected by pH (pH 3.0–9.5) for systems with fixed nanoparticle concentration of 0.15% w/v (Figure 3). For the control (TPP-0) when pH was 3.0, two peaks were detected: (i) $-7.8 \pm 4.4 \text{ mV}$, area = $88.7 \pm 6.3\%$; and (ii) $63.7 \pm 6.5 \text{ mV}$, area = $11.3 \pm 6.3\%$. The predominant population at about -7.8 mV supported the observed trend in ζ -potential for pH from 4.0 to ~ 6.8 , whereas a minor population had a significantly higher surface charge that may be the result of free CM- β -CD

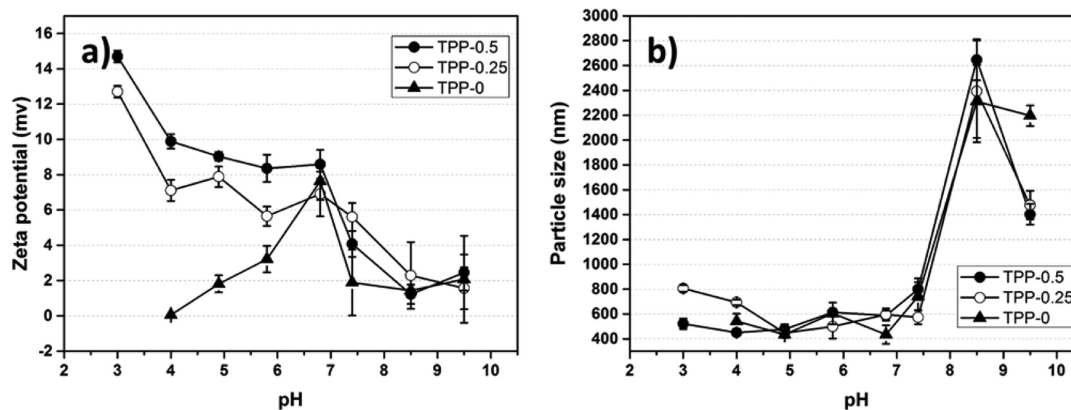


Figure 3. Effect of buffer pH value on nanoparticle (a) ζ -potential and (b) size for systems studied with a nanoparticle concentration of 0.15% w/v and $T = 25 \pm 1 \text{ }^\circ\text{C}$. Data points and error bars represent mean $\pm 1 \text{ S.D.}$, $n \geq 3$, and the lines are to guide the eye only.

and CS in solution. Because of the issues around the characterization of this system at this pH, these results were not included in the summary of results in Figure 3. TPP-0 showed a stepwise increase in ζ -potential from ~ 0 to ~ 8 mV as pH increased from 4.0 to 6.8. The ζ -potential increased with greater amounts of TPP (TPP-0.25, TPP-0.5), where TPP-0.5 had the highest ζ -potential of ~ 14 mV at pH of 3.0, which significantly decreased to ~ 9 mV at a pH 6.8 ($p < 0.001$). The ζ -potential for all three systems converged at ~ 9 mV when the pH approached 6.8. As the pH increased beyond 6.8, all three systems exhibited decreases in ζ -potential to ~ 2 mV at a pH of 9.5.

Nanoparticle size for all systems was also influenced by pH. The control system (TPP-0) at a pH of 3.0 yielded a single peak at 216.9 ± 9.8 nm, but these data were not included in the nanoparticle size results (Figure 3b) due to the issues surrounding the ζ -potential characterization. As the pH increased from 4.0 to 6.8, TPP-0 nanoparticles maintained a relatively constant size and varied between 435 and 605 nm (no significant difference between each point, $p > 0.05$). TPP-0.5 showed a similar trend in size as that of TPP-0 for pH values from 3.0–6.8. However, TPP-0.25 showed a decreasing trend in size from ~ 800 to ~ 450 nm (on average) as pH increased from 3.0 to 4.9 ($p < 0.001$). From pH 4.9–7.4, all systems exhibited similar trends in size, which started to increase as pH increased from 6.8 to 7.4. All systems showed a significant increase in particle size as the pH moved from 7.4 to 8.5: ~ 600 – 800 nm to ~ 2300 – 2650 nm (TPP-0, $p < 0.01$; TPP-0.25 and TPP-0.5, $p < 0.001$). A steep decrease in size to ~ 1500 nm occurred for both systems with TPP upon increasing pH from 8.4 to 9.5, whereas TPP-0 maintained a similar size of ~ 2200 nm.

3.2.3. Nanoparticle Characterization: Nanoparticle Stability. Nanoparticle stability in a physiological pH of 7.4 and a slightly acidic pH of 6.0 were chosen due to the fact that the amine group of chitosan has a $pK_a \approx 6.5$. The results summarized in Figure 4 illustrate that a solution pH less than the pK_a of chitosan led to a relatively stable nanoparticle size for all three systems of study. Regardless of the amount of TPP in the nanoparticle formulation, an initial diameter of ~ 500 – 600 nm decreased to 200–300 nm after 21 days of incubation in a solution with a pH of 6.0 (TPP-0 and TPP-0.25, $p < 0.05$; TPP-

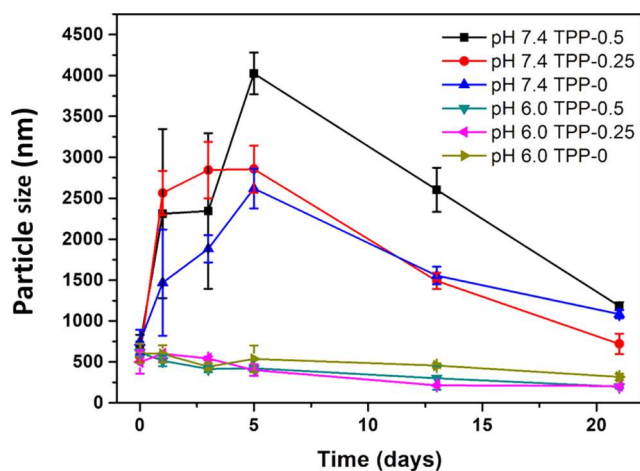


Figure 4. Nanoparticle stability in buffers at pH 6.0 and pH 7.4 as determined using the ζ sizer. Data represent mean \pm SD for $n \geq 3$ repeats, and lines are to guide the eye only.

0.5, $p < 0.001$). However, for pH 7.4, particle sizes drastically increased up to day 5, reached a maximum of ~ 5 – 8 -times greater than at day 0 ($p < 0.001$), and then all systems exhibited a decrease in particle size to near day 0 values (day 0 vs day 21: TPP-0, $p < 0.05$; TPP-0.25, $p > 0.05$; TPP-0.5, $p < 0.01$).

The impact of solution pH on the structure of nanoparticles was also measured using AFM. As shown in Figure 5, panels a–

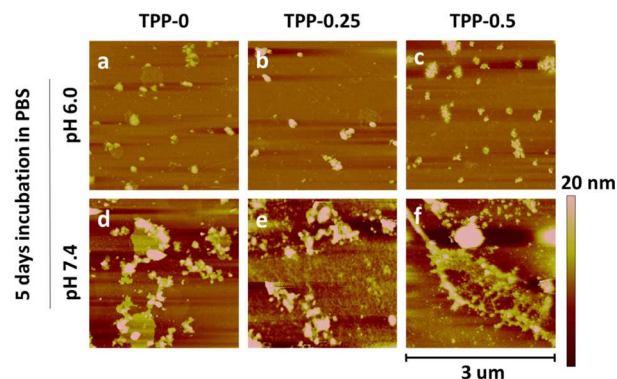


Figure 5. Representative AFM images of nanoparticles after 100 \times dilution: (a, d) TPP-0, (b, e) TPP-0.25, and (c, f) TPP-0.5. Incubated at 37 $^{\circ}$ C for 5 days in PBS at (a, b, c) pH 6.0 and (d, e, f) pH 7.4.

c, after 5 days of incubation in PBS at pH 6.0, distributed nanoparticles were observed in all groups. Deducting the radius of the AFM tip (8 nm) yielded an average measured diameter of TPP-0, TPP-0.25, and TPP-0.5 of around 201.8 ± 68.6 , 198.2 ± 42.4 , and 196.9 ± 65.8 nm, respectively ($n > 20$). However, after 5 days of incubation in PBS at pH 7.4 (Figure 5d–f), the morphology of nanoparticles changed dramatically: large aggregates were observed (>1000 nm) as well as insoluble amorphous clouds.

3.3. In Vitro Release of Dex from Nanoparticles. As shown in Figure 6, a burst release of 17–20% of loaded Dex occurred for all systems within 8 h. For the remainder of the systems at pH 6.0, there was only a slow but significant increase in release up to 18 days, which reached a cumulated release of $\sim 27\%$ ($p < 0.001$). However, systems incubated in pH 7.4 conditions showed further release after a 7 day lag period. At day 18 for these systems, release kinetics showed a significant

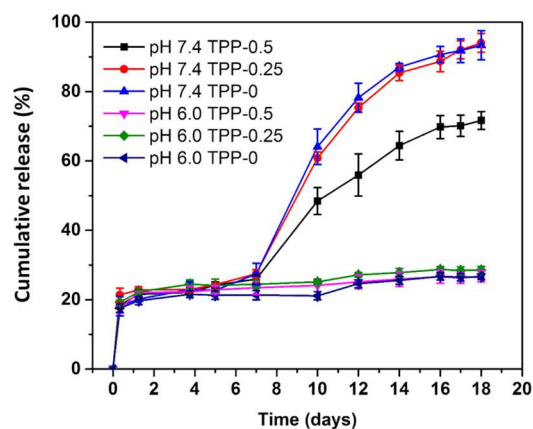


Figure 6. Cumulative release of Dex from nanoparticles with various TPP amounts in PBS at 37 $^{\circ}$ C and pH 6.0 or pH 7.4. Data represent mean \pm SD for $n \geq 3$ repeats, and lines are provided to guide the eye only.

increase from ~25–27% to as high ~93% for the TPP-0 and TPP-0.25 groups and ~72% for the TPP-0.5 group.

3.4. Effect of Nanoparticles on (RADA)₄ Self-Assembly. CD experiments were used to understand if the incorporation of nanoparticles would adversely affect the initial self-assembly of (RADA)₄ through analyzing the β -sheet peak, which is indicative of nanofiber formation (Figure 7, Table 2).

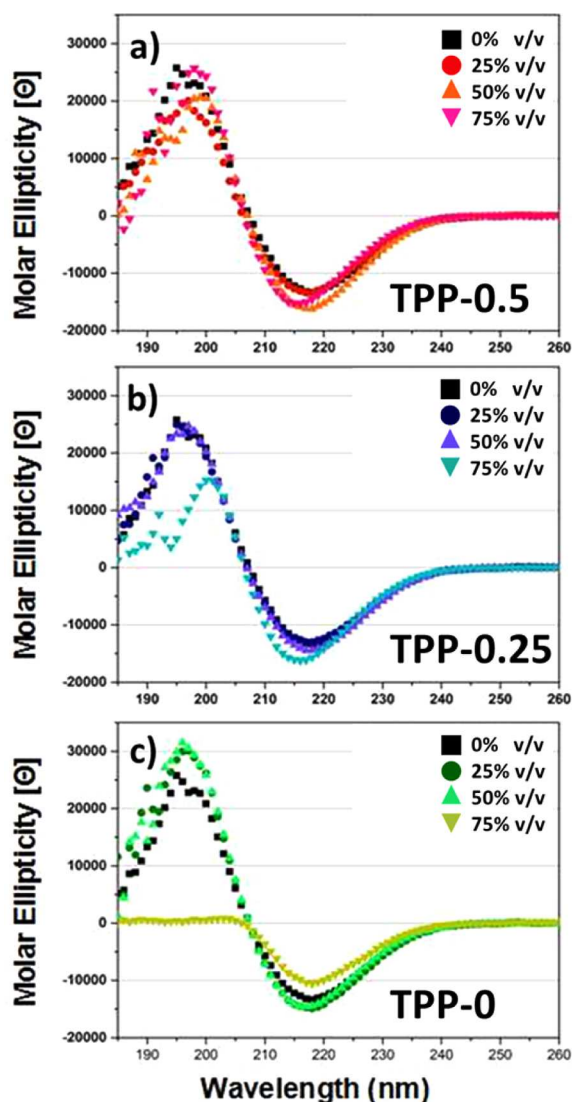


Figure 7. CD examination of the peptide structures of different mixing ratio of nanoparticles. The final concentrations of hydrogels are 0.5% w/v (RADA)₄ that contend 25–75% v/v nanoparticle stock solutions: (a) TPP-0.5, (b) TPP-0.25, and (c) TPP-0 suspensions in 5 mM PB. A typical CD spectrum of (RADA)₄ β -sheet structure contains a minimum at ~216 nm (β -sheet contents) and a maximum at 196 nm (the degree of β -sheet twist).⁴⁰ The nanoparticle solutions do not have absorption in CD examination, see Figure S2.

Control experiments were conducted using CD characterization of nanoparticles without the presence of (RADA)₄ (Supporting Information) where no response as a function of wavelength was observed. (RADA)₄ controls exhibited a typical β -sheet structure (minimum at 217–218 nm, maximum at 195–206 nm) for systems without nanoparticles (i.e., 0% v/v, or pure 0.5% (RADA)₄). This secondary structure content was further quantified using CDNN software (Table 2), which

yielded a high 46% (antiparallel + parallel) β -sheet content with low β -turn and random coil content of 11 and 27%, respectively. For all nanoparticle-(RADA)₄ systems, the β /TR ratio decreased dramatically from 1.20 as the ratio of nanoparticle stock solutions increased. In addition, the presence of TPP within the nanoparticles seemed to reduce the impact nanoparticles had on (RADA)₄ β -sheet formation (and thus on nanofiber formation). It is noteworthy that systems with 25% v/v nanoparticles were able to retain a peptide secondary structure similar to the control, illustrating that the nanofiber matrix was able to form.

3.5. In Vitro Release of Dex from Nanoparticle–Nanofiber Hydrogel Matrix. As shown in Figure 8, similar to the release profile of nanoparticles in buffer, there was also a burst release of Dex within the first ~12 h for all hybrid nanoscaffolds. The control CM- β -CD/Dex system showed a release of ~90% within 12 h, whereas a release of ~35–41% for pH 7.4 was almost double that of ~18–20% for pH 6.0 systems. Hybrid nanoscaffold systems at pH 7.4 exhibited an S-shaped release profile, with changes in release rates occurring at 12 h, 3 and 4 or 6 days depending on the system. Moreover, there is a tendency that the involvement of TPP leads to a slower release rate, a result also observed for release from nanoparticles in buffer without (RADA)₄. Furthermore, the involvement of TPP seemed to reduce the release rate for systems incubated in pH 7.4 solutions (Figure 8c). At the end of 8 days, all groups reached a plateau in cumulative release from 74% (TPP-0.5) to 95% (control). For the same systems incubated in PBS at pH 6.0, a very low level of drug release happened (~1.5%/day, Figure 8c) after a slight burst release within the first day. After 8 days of incubation, only 25.5% (TPP-0.5), 28.6% (TPP-0.25), and 30.7% (TPP-0) of total drug was released when incubated in pH 6.0 solution.

3.6. Hybrid Nanoscaffold Morphology. The in vitro release profiles for all hybrid systems showed a plateau in release after 5 days of incubation. To further understand the systems at this 5 day period, AFM characterization of the hybrid systems was conducted. AFM results for initially formed hybrid matrices with nanofibers and nanoparticles are summarized in Figure 9, panels a1–d1. Pure 0.5% w/v (RADA)₄ solutions exhibited long, evenly distributed, nanofibers (a1). Upon incorporation of nanoparticles without TPP (i.e., 25% v/v TPP-0 (b1)), it seemed that the nanofiber length overall was reduced compared to (RADA)₄ controls. However, upon incorporation of TPP containing nanoparticles (i.e., TPP-0.25 (c1) and TPP-0.5 (d1)), the nanofiber length was unchanged compared to (RADA)₄ controls. It also seemed that TPP-0.5 yielded a higher number of nanoparticles than compared to either TPP-0.25 or TPP-0 systems. This correlated with the results in Table 1, which show that the greatest yield of nanoparticles was observed for systems with TPP-0.5. In addition, before incubation, the interaction between nanoparticles and nanofibers was not obvious. Nanoparticles had a tendency to group but still remained isolated from nanofiber networks.

After 5 days of incubation, the morphology of the hybrid matrix changed dramatically, especially for TPP-0 and TPP-0.25 samples. For TPP-0 after incubation at pH 6.0 (b2), the network was made of short and stubby fibers, which may also resemble small particles (white small arrow). Meanwhile, fibers tended to aggregated at pH 7.4 (b3), and those short fibers also have a trend to be sequences of particles (white small arrow). The chitosan nanoparticles were hard to distinguish from fiber

Table 2. Estimated Structure Fractions of (RADA)₄ Peptide with Different Nanoparticles Contents at 25 °C

items	secondary-structure fractions (%)					total sum	β/TR^a
	helix	antiparallel	parallel	β -turn	random coil		
pure 0.5% (RADA) ₄	14.8	39.8	6.6	11.3	27.4	99.9	1.20
+25% v/v TPP-0	17.1	33.9	8.3	9.2	29.1	97.6	1.1
+50% v/v TPP-0	20.6	23.7	9.5	8.1	31.4	93.3	0.84
+75% v/v TPP-0	9.1	34.5	4.6	15.3	36.8	100.3	0.75
+25% v/v TPP-0.25	14.9	39.2	6.6	11.6	27.4	99.6	1.17
+50% v/v TPP-0.25	15.2	38.9	7.1	10.6	28.1	99.8	1.19
+75% v/v TPP-0.25	11.7	23.5	9.4	6.2	45.9	96.6	0.63
+25% v/v TPP-0.5	12.9	42.0	5.8	12.4	28.1	101.2	1.18
+50% v/v TPP-0.5	12.0	36.6	6.9	9.4	34.0	98.8	1.12
+75% v/v TPP-0.5	19.0	18.5	9.5	6.9	37.2	91.1	0.63

^a $\beta/TR = (\text{antiparallel} + \text{parallel})/(\beta\text{-turn} + \text{random coil})$. At the current state of the trained networks, the RMS error (%) for the prediction of one of these protein structures is ~ 2.07 .

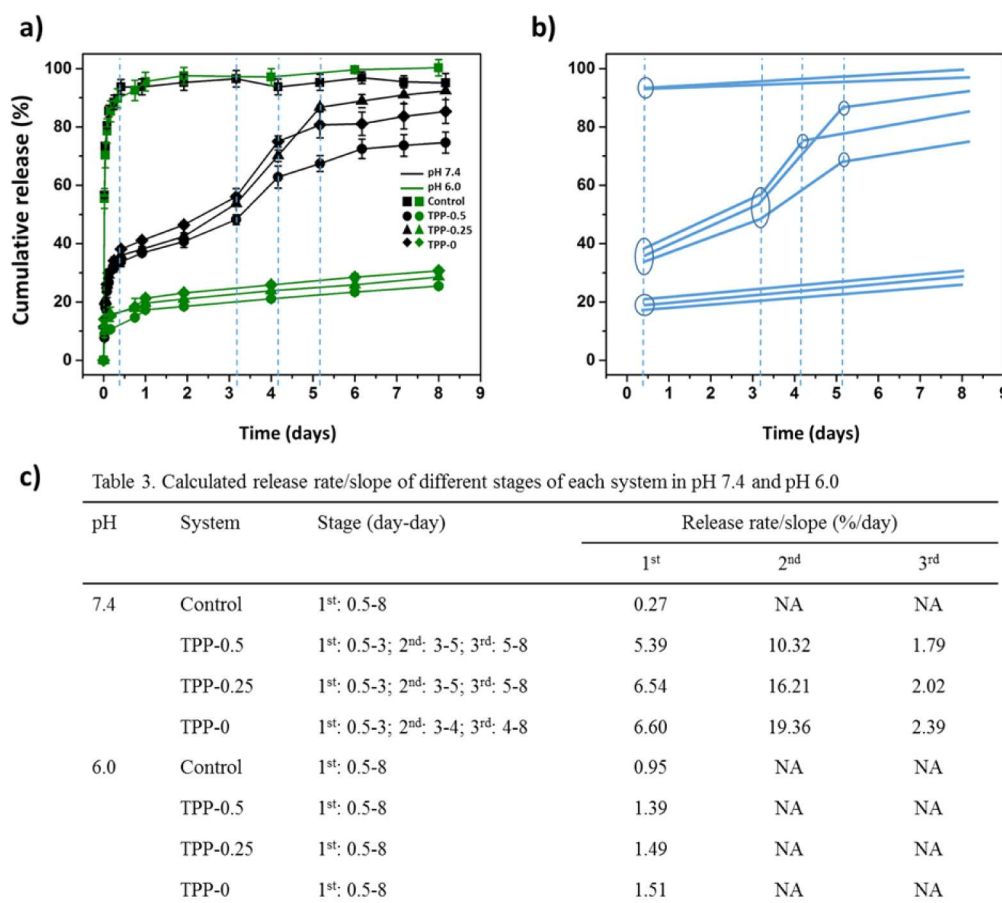


Figure 8. (a) Release profiles of Dex from hybrid matrix containing 0.5% w/v (RADA)₄ with 25% v/v nanoparticle stock solutions in PBS at pH 7.4 and pH 6.0, 37 °C. The control group is free release of CM- β -CD/Dex inclusion complex from 0.5% w/v (RADA)₄ gel. Data represent mean \pm SD for $n \geq 3$ repeats, and lines are to guide the eye only. (b) Sketch of different release stages. (c) Calculated release rate/slop of each release stage; the burst release at first 12 h was not included.

aggregates. For samples with TPP-0.25, there is no significant difference between pH 6.0 (c2) and pH 7.4 (c3) incubation, also shown as aggregates of broken short fibers, even particles-like fiber fragments. Similarly, it is hard to distinguish chitosan nanoparticles from fibers after incubation at pH 7.4. However, TPP-0.5 exhibited a better fiber compatibility than others. After being incubated with both pH 6.0 (d2) and pH 7.4 (d3), the fiber network looks very similar to pure (RADA)₄, namely fibers were long and relatively equally distributed. For pH 6.0 (d2), we can even see that chitosan nanoparticles were adhered

to nanofibers, not isolated from fibers network. After incubation at pH 7.4 (d3), regular shaped nanoparticles were barely observed. There are more thick bundles and fewer dispersed thin nanofibers in d3 compared with d2, which may due to the insolubilized nanoparticles.

The morphology change was obvious for the pure (RADA)₄ nanofiber matrix. After 5 days of incubation in pH 6.0, single nanofibers (a1) became fiber bundles (b1), and they cross-linked or branched into a complicated network. From the end of a branch of bundles (white arrow in a2), we can easily

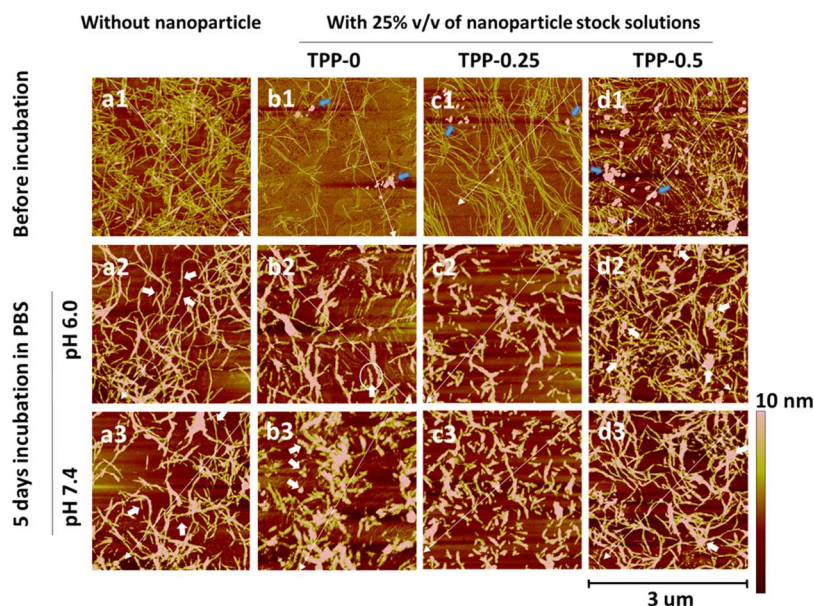


Figure 9. AFM images of hydrogels with 500-times dilution: (a1) 0.5% w/v (RADA)₄, (b1) 0.5% w/v (RADA)₄ with 25% v/v TPP-0 stock solution, (c1) 0.5% w/v (RADA)₄ with 25% v/v TPP-0.25 stock solution, and (d1) 0.5% w/v (RADA)₄ with 25% v/v TPP-0.5 stock solution. (a2–d2) Hydrogels incubated in PBS at pH 6.0 and 37 °C for 5 days. (a3–d3) Hydrogels incubated in PBS at pH 7.4 and 37 °C for 5 days. Small blue arrows point to nanoparticles. White arrows point out the cross-section height analyzed in Figure 10.

understand the thicker fibers were composed of single nanofibers, not single nanofibers that may be enlarged due to being coated with nanoparticle materials. Compared with b2, c2, and d2, it can be concluded that nanofiber can be broken into fragments by nanoparticles, and the increased TPP content inhibits this effect. After 5 days of incubation, no difference in fiber morphology could be discerned between pH 7.4 (a3) and pH 6.0 systems, where their effect was similar to perhaps more aggregations in b3.

The section heights of AFM measurement can provide more objective and intuitive data for analysis since the tip radius effect can be neglected and a number of random selected nanofiber section heights or diameters can be obtained. The cross-section information on each sample was shown in Figure 10, panel i. Each peak could be directly correlated to structures that were crossed by the diagonal white arrows in Figure 9. Nanoparticles can be easily distinguished from nanofibers before incubation. After incubation for 5 days, the fiber height increased dramatically at both pH 7.4 and pH 6.0. The statistical fiber heights were shown in Figure 10, panel ii, and the results indicate that before incubation the height of nanofiber is ~1.5 nm for all groups, which can be considered as single nanofiber. However, all nanofiber heights increased to 6.1–7.3 nm, except for TPP-0.5 pH 7.4 systems, which increased to 10.3 ± 3.8 nm. This height difference between TPP-0.5 (pH 7.4) was significantly higher than other groups (ii). Moreover, the distribution in cross-sectional height for each sample also changed, which can help us to understand the morphology change during different incubation environments.

4. DISCUSSION

Self-assembling peptide nanoscaffolds, like (RADA)₄, have unique features that make them amenable for a wide variety of tissue engineering scaffolds. That said, the release of hydrophobic drugs from these matrices has been an issue, particularly in maintaining the ability to self-assemble while maximizing the amount of drug loaded in the system.

As expected, Dex was successfully loaded in CS/CM-β-CD based nanoparticles via a CM-β-CD/Dex inclusion complex. It was confirmed that TPP plays an important role in chitosan nanoparticle formation, increasing both the nanoparticle yield and association with the nanoparticles. Although on average the Dex loading efficiency decreased with increasing TPP concentrations, a change that was not statistically significant. The total loaded amount of Dex was observed to be ~2%, which is well below the theoretical maximum mass ratios of Dex in TPP-0, TPP-0.25, and TPP-0.5 formulations of 4.5, 4.4, and 4.3%, respectively. Moreover, the stability of nanoparticles was significantly improved through TPP cross-linking. This is likely due to the fact that the pK_a of TPP is very low (i.e., negatively charged), and it has a relatively low molecular weight.⁴⁹

CS is a weak base (pK_a of ~6.5⁴⁴) that is soluble or not depending on the protonation of amino groups; thus, it is almost insoluble in aqueous solutions with pH > 7.0.^{50,51} In theory, the deprotonation of the amino groups at higher pH would lead to the disintegration of nanoparticles. In our work, a transition in particle size occurred in aqueous solutions at a pH ~7.4 where the particle sizes drastically increased from between 600 and 800 nm to 2300 and 2600 nm. This increase in size is likely due to particle aggregation, rather than particle growth,⁴⁹ brought on by a significant decrease in ζ-potential after a pH ~6.5. The decline in size at pH 9.5 may be due to the molecular dissociation of nanoparticles; specifically, the alkaline hydrolysis of TPP could break the nanoparticle structure of TPP-0.5 and TPP-0.25.^{52,53}

Relatively long-term stability of these nanoparticles was also influenced by pH. Incubation in pH 7.4 yielded particle sizes that rapidly over the first 5 days, whereas similar particles in pH 6.0 were relatively unchanged over the entire period of study (21 days). The low ζ-potential values for these particles when at pH 7.4 likely led to the increase in particle size through aggregation, which was observed in the AFM images taken after 5 days of incubation. In addition to aggregation, some

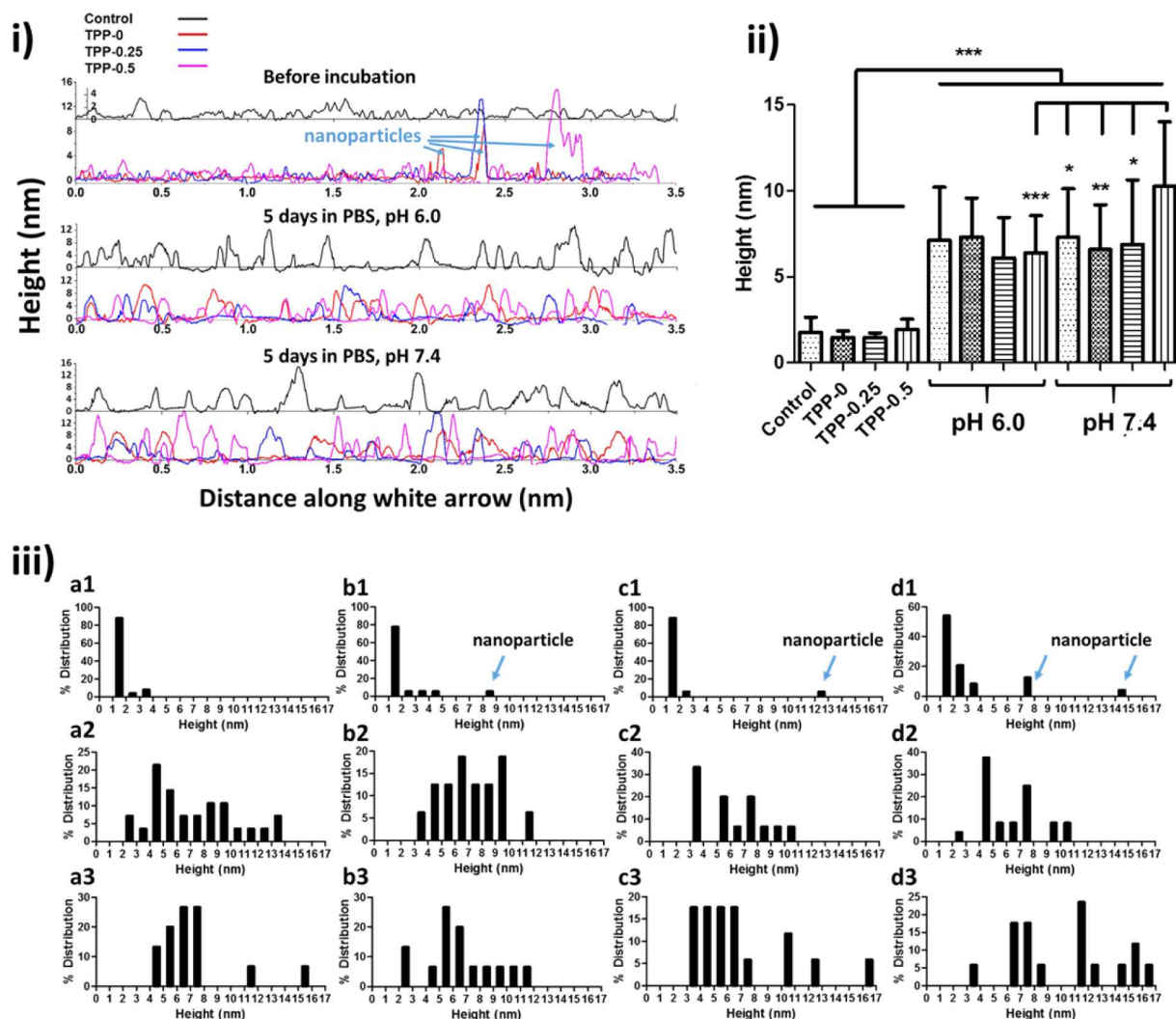


Figure 10. Measured section height of matrix networks: (i) height of cross-sections of “white arrows” for before incubation groups; white arrows that cross nanoparticles were selected for comparison. (ii) Average height of nanofibers before and after incubation in PBS for 5 days; nanoparticle heights in “before incubation” group were not included. (iii) Section height distributions of each sample analyzed. Data represent mean \pm SD for $n \geq 15$ repeats.

amorphous forms of material were also observed, which may be the presence of insoluble CS that has been dissociated from the particles. This may explain why the particle size eventually declined. The deprotonation of CS result in both particle aggregation and particle disassociation⁴⁹ may be because the hydrophobic property of deprotonation of CS and particle aggregation led to smaller surface area and then slowed down the imbibition or buffer absorption in the particles. Similar results were reported that after CS deprotonation: the particle aggregation kept ongoing, and the particle disassociation did not happen immediately.^{54,55}

The burst release for all particle systems in aqueous solution (Figure 6) may be due to the release of surface bound Dex or CM- β -CD/Dex complexes. Beyond this time point, all particles incubated in pH 6.0 buffer exhibited a very slow drug release. This may be due to the passive diffusion of Dex from particles rather than particle disassociation, which can be corresponded to the results in Figures 4 and 5. Interestingly, unlike other similar CS/CM- β -CD particle systems reported,³⁶ the deprotonation and disintegration in this nanoparticle did not cause a fast release in pH 7.4. This may be because, unlike reported deliveries of protein drugs, hydrophobic interactions between

dexamethasone released from inclusion complex and the insoluble chitosan may help in prolonging the release. Additionally, the aggregations of particles may lead to a smaller surface area that protects the loaded Dex from releasing into the environment and slow down the diffusion of the surrounding weakly alkaline buffer into the core of nanoparticles. As shown in Figure 4, after 5 days of incubation at pH 7.4, TPP-0.5 nanoparticles were at their largest size. That is, the surface area could be the smallest, thus explaining why it has the slowest release rate. In addition, the trend in decrease in particle size correlated to the release progress in Figure 6.

The incorporation of these particles into the self-assembling matrix should not hinder the initial self-assembly event. To understand this, the influence of incorporated particles on the resulting secondary structure of (RADA)₄ was studied using CD. The observation of the typical β -sheet structure for (RADA)₄ is currently deemed to be the gold-standard for indicating the formation of nanofibers and, thus, a successful self-assembly event. The control (RADA)₄ system yielded the expected trend in molar ellipticity. CD spectra (Figure 7) indicate that the amount and composition of nanoparticles added to the matrix may affect the β -sheet formation for

(RADA)₄. It was observed that the inclusion of particles to 50% v/v or less had no observable effect on nanofiber assembly as assessed via the CD spectra. That said, for TPP-0 and TPP-0.25, the typical β -sheet trend was altered, where the lack of TPP led to a greater decrease in β -twist signal. This may be due to the surface charge of the large number of particles in the matrix disrupting the ionic self-assembly of (RADA)₄. Those negatively charged residues of (RADA)₄ peptide may interact with positively charged CS and then prevent β -sheet and nanofiber structure. In all 25% v/v groups, a β -sheet content of 42–48% was observed, which was very similar to the control (RADA)₄ (46.4%). According to the study by Z. Ye and X. Zhao et al., the random coils and β -turn of (RADA)₄ via hydrogen or ionic bonds would directly affect the stability of the β -sheet and nanofibers.⁴⁰ Thus, it is necessary to compare the β -sheet content with the random coils and β -turn. On the basis of this, the β /TR ratios have been calculated and compared, which supported that 25% v/v nanoparticle solution in hydrogel did not drastically affect the assembly of (RADA)₄. In addition, it is worth mentioning that when interpreting the analysis of CD results (Table 2), the relative proportions, rather than the absolute content, is of major importance. AFM of matrices before incubation supports the above CD spectra in a more intuitive way. Even 25% v/v of nanoparticles solution has an effect on the nanofiber formation. Especially with TPP-0, the total amount of nanofibers decreased dramatically. Moreover, there is no other interaction between nanofiber and nanoparticles; nanoparticles are isolated from nanofiber networks.

In the *in vitro* release study of hybrid matrices, the control group was the free release of CM- β -CD/Dex inclusion complexes from 0.5% w/v (RADA)₄ gel. For an uncharged Dex or weakly charged CM- β -CD/Dex complex, there is a very fast release of free drug from this control group, which can be classified as a passive diffusion release. The result also proves that CM- β -CD and Dex do not interact with (RADA)₄ hydrogel matrix these conditions. Conversely, the Dex release profiles from the hybrid matrices showed an initial burst release followed by three relatively distinct regions of “zero order-like” release after 8 days. The burst release could be due to the release of surface-bound Dex. A trace of delayed release was also shown in the three groups. The very slow release profiles of samples under pH 6.0 correlated to the previous result in Figures 4 and 6. It seems that, for the hybrid system, CS deprotonation is the major determinant of drug release. As an injectable hydrogel, the solution pH is under the pK_a (~pH 6.5) of CS, and there is only a very slow drug release before injection. When the hydrogels meet with a physiological environment (pH 7.4), the three stages of sustained drug release occur, and the release rate may be controlled by altering the nanoparticle formula and content (Figure 8b,c).

To understand the mechanism of sustained drug release of the hydrogel matrix, the morphologies after incubation at different pH were obtained by AFM. As we can conclude from previous results, matrix formation at day 5 is typical. Not only can the day 5 images correlate with previous images of nanoparticles, but also day 5 is a late stage of drug release of hydrogels. After 5 days of incubation at pH 6.0, the hydrogel with TPP-0 seemed to be composed of short stubby fibers. This may be due to the surface charged nanoparticles interfering with the nanofiber stability. This effect was reduced upon increasing TPP content. TPP-0.5 systems at pH 6.0 (Figure 9d2) showed almost the same matrix morphology as the pure (RADA)₄, and nanoparticles were interacting with fiber

bundles, which means that not only the interaction between each fibers became stronger during the incubation in PBS, but also the interaction between nanofibers and nanoparticles became more significant. After pH 7.4 incubation, unlike nanoparticles in PBS without (RADA)₄, no big particle aggregations can be found (Figure 5b3,c3,d3) in those hybrid matrices. This may explain why the *in vitro* release profiles of hybrid matrices (Figure 8a) have no significant delay effect and a much more rapid release compared with release profiles of nanoparticles themselves (Figure 6). Nanoparticle aggregation progress may have been inhibited by the scaffold networks, insoluble particles being covered by peptide fibers, which prevent further aggregation. The structured networks may help nanoparticles remain isolated from each other and thus increase the surface area of the total particles in the matrix and thus alter the release kinetics. The TPP-0.5 nanoparticle led to more and thicker fiber bundles than others (Figure 10ii,iii), which can explain why this matrix has the slowest release rate at pH 7.4.

5. CONCLUSION

Dex has been successfully loaded in CS-based nanoparticles via the formation of CM- β -CD/Dex inclusion complexes. The deionization of CS in physiological environment led to an aggregation and dissociation of solution free nanoparticles, which resulted in a delayed and sustained release, while the particle is stable in size with a very slow release at pH 6.0 for several days. Nanoparticle cross-linking by TPP improved the drug loading and yield and induced a more dramatic pH response, which slowed down the release rate due to the formation of aggregates that reduced the apparent nanoparticle surface area for release to occur. The peptide self-assembly nanofiber is affected by the concentration and the type of nanoparticle dramatically before and after incubation. Formulas with 25% v/v nanoparticle solution were observed to not alter the secondary structure of (RADA)₄ nanofibers. The nanofiber and nanoparticles aggregate into hybrid bundle networks, which explained why drug release from hybrid system achieved a faster and less delayed release. However, the stabilities of each hybrid systems are different after 5 days of incubation. TPP presence affects the hybrid matrix morphology and further affects the release rates for these systems. It is thought that this self-assembling system may provide a platform for drug delivery from peptide-based nanoscaffolds.

■ ASSOCIATED CONTENT

Supporting Information

The Supporting Information is available free of charge on the ACS Publications website at DOI: 10.1021/acs.biomac.6b00040.

Chemical structures of CS, CM- β -CD, TPP, and Dex; original CD spectra of matrix and nanoparticle stock solution (PDF)

■ AUTHOR INFORMATION

Corresponding Author

*Phone: +1(780) 492 6020. Fax: +1(780) 492 2881. E-mail: larry.unsworth@ualberta.ca.

Notes

The authors declare no competing financial interest.

ACKNOWLEDGMENTS

This work was supported by Women's Children's Health Research Initiative, NSERC (Canada), NINT-NRC. L.L. is supported by a grant from the China Scholarship Council (CSC). The authors gratefully acknowledge Paul Concepcion, Mike Xia, and Aditi Saini for useful and valuable suggestions during the work.

REFERENCES

- (1) Branco, M. C.; Schneider, J. P. Self-assembling materials for therapeutic delivery. *Acta Biomater.* **2009**, *5* (3), 817–831.
- (2) Matson, J. B.; Stupp, S. I. Self-assembling peptide scaffolds for regenerative medicine. *Chem. Commun.* **2012**, *48* (1), 26–33.
- (3) Gelain, F.; Horii, A.; Zhang, S. G. Designer self-assembling peptide scaffolds for 3-D tissue cell cultures and regenerative medicine. *Macromol. Biosci.* **2007**, *7* (5), 544–551.
- (4) Hoare, T. R.; Kohane, D. S. Hydrogels in drug delivery: Progress and challenges. *Polymer* **2008**, *49* (8), 1993–2007.
- (5) Gou, M. L.; Li, X. Y.; Dai, M.; Gong, C. Y.; Wang, X. H.; Xie, Y.; Deng, H. X.; Chen, L. J.; Zhao, X.; Qian, Z. Y.; Wei, Y. Q. A novel injectable local hydrophobic drug delivery system: Biodegradable nanoparticles in thermo-sensitive hydrogel. *Int. J. Pharm.* **2008**, *359* (1–2), 228–233.
- (6) Peng, K.; Tomatsu, I.; Korobko, A. V.; Kros, A. Cyclodextrin-dextran based in situ hydrogel formation: a carrier for hydrophobic drugs. *Soft Matter* **2010**, *6* (1), 85–87.
- (7) Yu, L.; Ding, J. D. Injectable hydrogels as unique biomedical materials. *Chem. Soc. Rev.* **2008**, *37* (8), 1473–1481.
- (8) Yokoi, H.; Kinoshita, T.; Zhang, S. G. Dynamic reassembly of peptide RADA16 nanofiber scaffold. *Proc. Natl. Acad. Sci. U. S. A.* **2005**, *102* (24), 8414–8419.
- (9) Zhang, S. G.; Gelain, F.; Zhao, X. J. Designer self-assembling peptide nanofiber scaffolds for 3D tissue cell cultures. *Semin. Cancer Biol.* **2005**, *15* (5), 413–420.
- (10) Zhang, S. G. Fabrication of novel biomaterials through molecular self-assembly. *Nat. Biotechnol.* **2003**, *21* (10), 1171–1178.
- (11) Zhang, S. G. Emerging biological materials through molecular self-assembly. *Biotechnol. Adv.* **2002**, *20* (5–6), 321–339.
- (12) Wang, X. M.; Horii, A.; Zhang, S. G. Designer functionalized self-assembling peptide nanofiber scaffolds for growth, migration, and tubulogenesis of human umbilical vein endothelial cells. *Soft Matter* **2008**, *4* (12), 2388–2395.
- (13) Liu, X.; Wang, X. M.; Horii, A.; Wang, X. J.; Qiao, L.; Zhang, S. G.; Cui, F. Z. In vivo studies on angiogenic activity of two designer self-assembling peptide scaffold hydrogels in the chicken embryo chorioallantoic membrane. *Nanoscale* **2012**, *4* (8), 2720–2727.
- (14) Kim, J. H.; Jung, Y.; Kim, B. S.; Kim, S. H. Stem cell recruitment and angiogenesis of neuropeptide substance P coupled with self-assembling peptide nanofiber in a mouse hind limb ischemia model. *Biomaterials* **2013**, *34* (6), 1657–1668.
- (15) Pan, H. T.; Hao, S. F.; Zheng, Q. X.; Li, J. F.; Zheng, J.; Hu, Z. L.; Yang, S. H.; Guo, X. D.; Yang, Q. Bone induction by biomimetic PLGA copolymer loaded with a novel synthetic RADA16-P24 peptide in vivo. *Mater. Sci. Eng., C* **2013**, *33* (6), 3336–3345.
- (16) Horii, A.; Wang, X. M.; Gelain, F.; Zhang, S. G. Biological Designer Self-Assembling Peptide Nanofiber Scaffolds Significantly Enhance Osteoblast Proliferation, Differentiation and 3-D Migration. *PLoS One* **2007**, *2* (2), e190.
- (17) Zou, Z. W.; Zheng, Q. X.; Wu, Y. C.; Guo, X. D.; Yang, S. H.; Li, J. F.; Pan, H. T. Biocompatibility and bioactivity of designer self-assembling nanofiber scaffold containing FGL motif for rat dorsal root ganglion neurons. *J. Biomed. Mater. Res., Part A* **2010**, *95A* (4), 1125–1131.
- (18) Zou, Z. W.; Liu, T.; Li, J. F.; Li, P. D.; Ding, Q.; Peng, G.; Zheng, Q. X.; Zeng, X. L.; Wu, Y. C.; Guo, X. D. Biocompatibility of functionalized designer self-assembling nanofiber scaffolds containing FRM motif for neural stem cells. *J. Biomed. Mater. Res., Part A* **2014**, *102* (5), 1286–1293.
- (19) Gelain, F.; Unsworth, L. D.; Zhang, S. G. Slow and sustained release of active cytokines from self-assembling peptide scaffolds. *J. Controlled Release* **2010**, *145* (3), 231–239.
- (20) Guo, H. D.; Cui, G. H.; Yang, J. J.; Wang, C.; Zhu, J.; Zhang, L. S.; Jiang, J.; Shao, S. J. Sustained delivery of VEGF from designer self-assembling peptides improves cardiac function after myocardial infarction. *Biochem. Biophys. Res. Commun.* **2012**, *424* (1), 105–111.
- (21) Koutsopoulos, S.; Zhang, S. G. Two-layered injectable self-assembling peptide scaffold hydrogels for long-term sustained release of human antibodies. *J. Controlled Release* **2012**, *160* (3), 451–458.
- (22) Nagai, Y.; Unsworth, L. D.; Koutsopoulos, S.; Zhang, S. G. Slow release of molecules in self-assembling peptide nanofiber scaffold. *J. Controlled Release* **2006**, *115* (1), 18–25.
- (23) Liu, J. P.; Zhang, L. L.; Yang, Z. H.; Zhao, X. J. Controlled release of paclitaxel from a self-assembling peptide hydrogel formed in situ and antitumor study in vitro. *Int. J. Nanomed.* **2011**, *6*, 2143–2153.
- (24) Fung, S. Y.; Yang, H.; Chen, P. Sequence Effect of Self-Assembling Peptides on the Complexation and In Vitro Delivery of the Hydrophobic Anticancer Drug Ellipticine. *PLoS One* **2008**, *3* (4), e1956.
- (25) Fung, S. Y.; Yang, H.; Bhola, P. T.; Sadatmousavi, P.; Muzar, E.; Liu, M. Y.; Chen, P. Self-Assembling Peptide as a Potential Carrier for Hydrophobic Anticancer Drug Ellipticine: Complexation, Release and In Vitro Delivery. *Adv. Funct. Mater.* **2009**, *19* (1), 74–83.
- (26) Altunbas, A.; Lee, S. J.; Rajasekaran, S. A.; Schneider, J. P.; Pochan, D. J. Encapsulation of curcumin in self-assembling peptide hydrogels as injectable drug delivery vehicles. *Biomaterials* **2011**, *32* (25), 5906–5914.
- (27) Hong, Y. S.; Legge, R. L.; Zhang, S.; Chen, P. Effect of amino acid sequence and pH on nanofiber formation of self-assembling peptides EAK16-II and EAK16-IV. *Biomacromolecules* **2003**, *4* (5), 1433–1442.
- (28) Lakshmanan, A.; Zhang, S. G.; Hauser, C. A. E. Short self-assembling peptides as building blocks for modern nanodevices. *Trends Biotechnol.* **2012**, *30* (3), 155–165.
- (29) Keyes-Baig, C.; Duhamel, J.; Fung, S. Y.; Bezaire, J.; Chen, P. Self-assembling peptide as a potential carrier of hydrophobic compounds. *J. Am. Chem. Soc.* **2004**, *126* (24), 7522–7532.
- (30) Haines-Butterick, L.; Rajagopal, K.; Branco, M.; Salick, D.; Rughani, R.; Pilarz, M.; Lamm, M. S.; Pochan, D. J.; Schneider, J. P. Controlling hydrogelation kinetics by peptide design for three-dimensional encapsulation and injectable delivery of cells. *Proc. Natl. Acad. Sci. U. S. A.* **2007**, *104* (19), 7791–7796.
- (31) Branco, M. C.; Pochan, D. J.; Wagner, N. J.; Schneider, J. P. The effect of protein structure on their controlled release from an injectable peptide hydrogel. *Biomaterials* **2010**, *31* (36), 9527–9534.
- (32) Zhang, L.; Gu, F. X.; Chan, J. M.; Wang, A. Z.; Langer, R. S.; Farokhzad, O. C. Nanoparticles in medicine: Therapeutic applications and developments. *Clin. Pharmacol. Ther.* **2008**, *83* (5), 761–769.
- (33) Cho, K. J.; Wang, X.; Nie, S. M.; Chen, Z.; Shin, D. M. Therapeutic nanoparticles for drug delivery in cancer. *Clin. Cancer Res.* **2008**, *14* (5), 1310–1316.
- (34) Banerjee, S. S.; Chen, D. H. Magnetic nanoparticles grafted with cyclodextrin for hydrophobic drug delivery. *Chem. Mater.* **2007**, *19* (25), 6345–6349.
- (35) Strong, L. E.; Dahotre, S. N.; West, J. L. Hydrogel-nanoparticle composites for optically modulated cancer therapeutic delivery. *J. Controlled Release* **2014**, *178*, 63–68.
- (36) Krauland, A. H.; Alonso, M. J. Chitosan/cyclodextrin nanoparticles as macromolecular drug delivery system. *Int. J. Pharm.* **2007**, *340* (1–2), 134–42.
- (37) Teixeira-Osorio, D.; Remunan-Lopez, C.; Alonso, M. J. New Generation of Hybrid Poly/Oligosaccharide Nanoparticles as Carriers for the Nasal Delivery of Macromolecules. *Biomacromolecules* **2009**, *10* (2), 243–249.
- (38) Ammar, H. O.; El-Nahhas, S. A.; Ghorab, M. M.; Salama, A. H. Chitosan/cyclodextrin nanoparticles as drug delivery system. *J. Inclusion Phenom. Mol. Recognit. Chem.* **2012**, *72* (1–2), 127–136.

- (39) Teijeiro-Osorio, D.; Remunan-Lopez, C.; Alonso, M. J. Chitosan/cyclodextrin nanoparticles can efficiently transfect the airway epithelium in vitro. *Eur. J. Pharm. Biopharm.* **2009**, *71* (2), 257–263.
- (40) Ye, Z. Y.; Zhang, H. Y.; Luo, H. L.; Wang, S. K.; Zhou, Q. H.; Du, X. P.; Tang, C. K.; Chen, L. Y.; Liu, J. P.; Shi, Y. K.; Zhang, E. Y.; Ellis-Behnke, R.; Zhao, X. J. Temperature and pH effects on biophysical and morphological properties of self-assembling peptide RADA16–1. *J. Pept. Sci.* **2008**, *14* (2), 152–162.
- (41) Sabadini, E.; Cosgrove, T.; Egidio, F. C. Solubility of cyclomaltooligosaccharides (cyclodextrins) in H₂O and D₂O: a comparative study. *Carbohydr. Res.* **2006**, *341* (2), 270–274.
- (42) Barnes, P. J. Corticosteroids: The drugs to beat. *Eur. J. Pharmacol.* **2006**, *533* (1–3), 2–14.
- (43) Brewster, M. E.; Loftsson, T. Cyclodextrins as pharmaceutical solubilizers. *Adv. Drug Delivery Rev.* **2007**, *59* (7), 645–666.
- (44) Domard, A. pH and c.d. measurements on a fully deacetylated chitosan: application to CuII–polymer interactions. *Int. J. Biol. Macromol.* **1987**, *9* (2), 98–104.
- (45) Bourlard, H.; Morgan, N.; Wooters, C.; Renals, S. C. Context Dependent Neural Network for Continuous Speech Recognition. *Int. Conf. Acoust. Spee* **1992**, B349–B352.
- (46) Mi, F.-L.; Shyu, S.-S.; Lee, S.-T.; Wong, T.-B. Kinetic study of chitosan-tripolyphosphate complex reaction and acid-resistive properties of the chitosan-tripolyphosphate gel beads prepared by in-liquid curing method. *J. Polym. Sci., Part B: Polym. Phys.* **1999**, *37* (14), 1551–1564.
- (47) Martins, A. F.; de Oliveira, D. M.; Pereira, A. G.; Rubira, A. F.; Muniz, E. C. Chitosan/TPP microparticles obtained by microemulsion method applied in controlled release of heparin. *Int. J. Biol. Macromol.* **2012**, *51* (5), 1127–33.
- (48) Luo, Y.; Zhang, B.; Cheng, W.-H.; Wang, Q. Preparation, characterization and evaluation of selenite-loaded chitosan/TPP nanoparticles with or without zein coating. *Carbohydr. Polym.* **2010**, *82* (3), 942–951.
- (49) Gan, Q.; Wang, T.; Cochrane, C.; McCarron, P. Modulation of surface charge, particle size and morphological properties of chitosan-TPP nanoparticles intended for gene delivery. *Colloids Surf., B* **2005**, *44* (2–3), 65–73.
- (50) Denuziere, A.; Ferrier, D.; Domard, A. Chitosan-chondroitin sulfate and chitosan-hyaluronate polyelectrolyte complexes. Physicochemical aspects. *Carbohydr. Polym.* **1996**, *29* (4), 317–323.
- (51) Piron, E.; Accominotti, M.; Domard, A. Interaction between Chitosan and Uranyl Ions. Role of Physical and Physicochemical Parameters on the Kinetics of Sorption. *Langmuir* **1997**, *13* (6), 1653–1658.
- (52) Bell, R. N. Hydrolysis of dehydrated sodium phosphates. *Ind. Eng. Chem.* **1947**, *39* (2), 136–140.
- (53) Thilo, E.; Wieker, W. Study of degradation of polyphosphates in aqueous solution. *J. Polym. Sci.* **1961**, *53* (158), 55–59.
- (54) López-León, T.; Carvalho, E. L. S.; Seijo, B.; Ortega-Vinuesa, J. L.; Bastos-González, D. Physicochemical characterization of chitosan nanoparticles: electrokinetic and stability behavior. *J. Colloid Interface Sci.* **2005**, *283* (2), 344–351.
- (55) Nimesh, S.; Thibault, M.; Lavertu, M.; Buschmann, M. Enhanced Gene Delivery Mediated by Low Molecular Weight Chitosan/DNA Complexes: Effect of pH and Serum. *Mol. Biotechnol.* **2010**, *46* (2), 182–196.